

Load Alleviation on Wind Turbine Blades using Variable Airfoil Geometry

Peter Bjørn Andersen, Mac Gaunaa, Christian Bak and Thomas Buhl
Wind Energy Department, Risø National Laboratory, P.O. Box 49, DK 4000, Denmark
email peter.bjorn.andersen@risoe.dk

Abstract:

Dynamically deformable trailing edge (TE) flaps have been modeled on a 33 meter long V66 blade from Vestas. The structural blade model comprises a modal expansion of a cantilever beam with the effects of TE deformations added. The aerodynamic model includes a BEM model with 3D corrections and a two dimensional model which includes the unsteady effect of the deforming trailing edge. A proportional differential (PD) control using the local flapwise deflection is implemented to control the flaps. Effects of system time lag, flap power consumption and signal noise are included.

The equivalent flapwise blade root moment is reduced 60% for inflow with 10% turbulence using 7 meter TE flaps where actuators consume 100W/m at maximum consumption rate. The potential is reduced to 40% when signal noise is added to the control.

Keywords: Wind Turbine, Load Alleviation, Fatigue Loads, Trailing Edge Flaps, PID control, Signal Noise.

1 Introduction

Wind turbine blades are subject to fast fluctuating loads during operation due to turbulence, operation in yawed conditions, shear flow and tower shadowing effects. These fluctuating loads cause structural fatigue damage. Previously, effort have been put on using the conventional pitch system of wind turbines to alleviate fluctuating loads using cyclic or individual pitch control schemes [1,2]. However, the speed by which the servo pitches the blade is limited by the inertia of the full blade. For fast pitching motions the structural dynamics of the blade plays a role as the turning motion propagates from the root towards the tip of the blade. It is not likely that all fluctuations can ever be compensated by a blade pitching control system, as the fluctuations are a function of the rotor radius due to the turbulent structures in the wind. Also, as the rotor diameter increases there will be less correlation between the turbulent structures from e.g. the bottom part of the rotor and the top part of the rotor. The potential for reducing the load in an

equivalent 2D aeroelastic system equipped with adaptive trailing edge geometry was investigated by Buhl et al. [3] which showed that the load reduction potential was significant. The work described in this paper is part of the ADAPWING project funded by the Danish Research Council.

The ADAPWING project overview is available at <http://www.risoe.dk/vea/adapwing>.

The ultimate goal within load reduction using adaptive TE geometry is to eliminate all fluctuating aerodynamic loads. However, this is not obtainable due to constraints imposed by control strategy, signal noise, actuator power consumption, time lag, etc. The purpose of the present study is to quantify the potential of reducing the equivalent flapwise blade root moment by use of deformable TE geometry on a Vestas V66 wing mounted on a rigid wind turbine.

The TE geometry is deformed using spanwise individually controlled PD regulators, one for each aerodynamic evaluation point in the aeroservoelastic algorithm. Parameter studies by Andersen [4] and Buhl et al. [3] showed that the optimum TE deflection angle of the airfoil camberline correlates well with the relative flapwise deflection of the blade close to the flap. This effectively corresponds to a system that is continuously controlled along the outer 11 meters of the wing span. Hence, the control input parameter for the individual PD regulators is the local flapwise deflections of the wing. The object function is the reduction in the equivalent blade root moments.

The investigation is carried out using an aeroelastic model of a three blade system with infinitely stiff main shaft and tower, but with full modeling of the structural dynamics of the blades.

2 Method

The aeroservoelastic system is approximated by coupling a model for the unsteady aerodynamic response, a model for the structural response and a model for the control behavior of the deformable trailing edge. The parameters for the controls are optimized using an iterative gain tuning method for

each of the six airfoil section with TE deformable geometry. The object function is the minimization of the equivalent flapwise blade root moment.

Figure 1 shows the V66 wing with the outermost 11m deformable TE part highlighted.

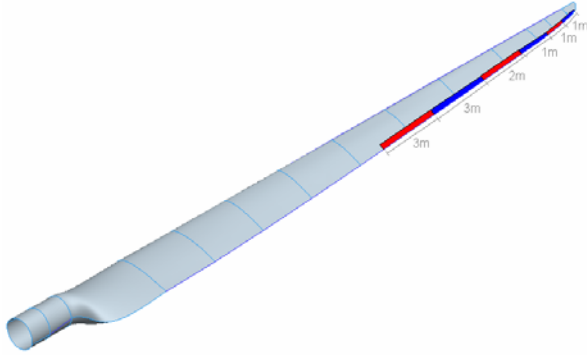


Figure 1: The V66 wing with the deformable TE geometry marked on the outer part of the wing.

The optimal shape for the TE deformable geometry was investigated by Trolborg [17] using the CFD code EllipSys2D. The study concluded that the use of rigid trailing edge flaps is not plausible due to the added noise and loss in driving force associated with separation due to very small surface curvature ratios at the junction between the airfoil and the rigid flap. Therefore, the idea of using adaptive TE geometry or non-rigid flaps on wind turbines arises. Figure 2 illustrates the flapping geometry represented by the deformed camberline.

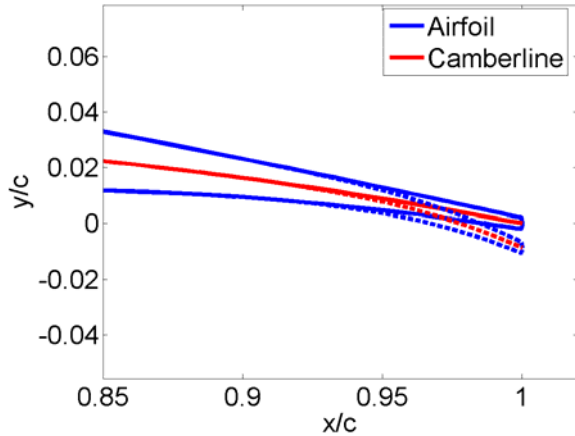


Figure 2: Airfoil camberline with deformable TE geometry, where 'x/c' indicates the chord length.

Actuating the last 10% of the camberline gave prudent cost/benefit characteristics. A relative small change in the 10% TE geometry caused a large shift in lift characteristics without introducing a significant increase in drag. The TE deformable geometry can deflect within the range from -5 to 5 degrees, where the 5 degree deflection is shown in Figure 2 in comparison to the undeformed airfoil shape. The

deflection angle is given by the angle between the lines starting at 90% chord to the TE point at 100% chord.

2.1 Aerodynamic model

The main part of the aerodynamic model used in this work is similar to most aeroelastic prediction tools, with the unsteady aerodynamic effect of the deformable TE added. Prandtl's tip-loss factor [5] is applied to the implemented unsteady BEM model. The rotational speed of the blade (ω) is held constant at 19.8rpm. The relative wind speed at each section is given by the vector equation (1)

$$\underline{V}_{rel} = \underline{V}_{wind} + \underline{V}_{rot} + \underline{W} + \underline{V}_{defl} \quad (1)$$

, where \underline{V}_{rel} is the relative wind speed seen by the blade at a given radial position, \underline{V}_{wind} marks the undisturbed wind speed, \underline{V}_{rot} the rotational wind speed, \underline{V}_{defl} the contribution from the deflection of the blade and \underline{W} the induced velocity of the rotating blade. The quasi-stationary wake is modeled using Bramwell's [6] derivation of Glauert's relation between thrust and the induced velocity, and the dynamics of the rotor wake is modelled using an inflow model called TUDk [7].

The addition to the standard aeroelastic model is the treatment of the dynamic aerodynamic forces due to the arbitrary motion and inflow to the airfoil sections of varying shape. The aerodynamic loads are added to the model in a slightly different way than usually done for unsteady BEM models. Normally the angle of attack is found based on the relative wind speed which is used to lookup lift, drag and torsion. In our case the profile data becomes a function of angle of attack (α) and flap deflection (β). Furthermore, the well known effects like the tip-vortex will be joined by new unsteady dynamic wake effects from flapping. Theodorsen [11] separates the forces of motion from the forces of the unsteady wake. In the work of Gaunaa [18], the flat plate of Theodorsen has been replaced by a series of shape functions describing the camberline and the motion of the flap including the effect of the dynamic wake while flapping. The output from the Gaunaa model is a pressure difference distribution over the airfoil, from which other quantities like forces, moments and power consumption are obtained in analytical form. The dynamic effects linked to the thickness distribution are simulated by altering the classic response functions. The potential flow model does not take viscous effects into account.

The aerodynamic forces on the airfoil is found using equation (2)

$$F = F_{steady,table}(\alpha) + F_{flap}(\alpha, \beta) \quad (2)$$

Equation (2) expresses the forces locally on the airfoil as a sum of steady profile data ($F_{steady,table}$) and the partially unsteady part from the potential flow model (F_{flap}), which, in reality shifts the offset of the steady profile curve and includes the unsteady wake effects of flapping. The procedure is only valid for the linear part of the original profile data well before stall where there is a linear relation between α and lift.

2.2 Structural model

The method described by Hansen [8] determines the eight shape functions (4 flap, 2 edge, 2 torsion) used to describe the deflections of the V66 blade. The motion is described by a second order system shown in equation (3)

$$\underline{M}\ddot{\underline{X}} + \underline{D}\dot{\underline{X}} + \underline{K}\underline{X} = \underline{F} \quad (3)$$

, where \underline{M} \underline{D} \underline{K} are diagonal mass, damping and stiffness matrixes, \underline{X} the generalized coordinates of deformation and \underline{F} the generalized force which includes the virtual work performed by exterior aerodynamic and fictitious forces for each of the eight Degrees Of Freedom (DOF) one for each shape function. The structural damping coefficients are constant and given by Hansen [9]. The centrifugal stiffening is implemented as described by Øye [10]. The deformable TE geometry deforms the last 10% of the camberline shown in Figure 2 and weighs 1% of the cross sectional mass, and the inertial forces linked to the relative acceleration of this mass are treated as in the two dimensional case described in Buhl et al. [3].

2.3 Servo model

A PD control is used to find the needed deflection angle (β) as described by equation (4), based on the flapwise deflection of the section (y). The reference deflection is integrated over a period (τ) of 1P.

$$\beta = Kp \left(y - \frac{1}{\tau} \int_{t-\tau}^t y dt \right) + Kd \dot{y} \quad (4)$$

The forces of inertia prohibits the flaps from responding instantly. Both during flap acceleration and deceleration the control must avoid overshooting the needed deflection angle. Kp marks the constant proportional gain and Kd the differential gain. The needed power (P) for the flap servo motor is given by an inner PD regulator and must balance the effect of inertia and aerodynamic, see equation (5):

$$P + P_{inertia} + P_{aerodynamic} = 0 \quad (5)$$

The aerodynamic effect is given by Gaunaa[18], whereas the inertial effect is described by Andersen [4]. The flap actuator control is seeking to minimize the error (E_{pwr}) between the real deflection angle

(β_{real}) and the needed deflection angle, see equation (6).

$$E_{pwr} = \beta - \beta_{real} \quad (6)$$

The actuator PID power regulator determines the needed power by equation (7):

$$P = Kp \cdot E_{pwr} + Ki \int E_{pwr} dt + Kd \cdot \dot{E}_{pwr} \quad (7)$$

where Kp, Ki and Kd marks the constant proportional, integral and differential gain respectively.

2.4 Fatigue

The theory of equivalent loads is used to measure fatigue. A 10 minute time series of the flapwise root moment is transformed into a single equivalent load (E_{QF}). This method reduces the complexity of comparing two time series to comparing two equivalent root moments. The rain flow counting method described by Kensche [12] is used.

2.5 Iterative gain tuning

A multi layer method is used to iteratively determine the optimal gains for each of the flapping sections. The gains are adjusted in an iterative manner in a loop starting with the section closest to the root and adding one section at a time towards the top. For each new section added new gains are predicted by minimizing the equivalent flapwise blade root moment.

2.6 Signal noise model

Signal noise is simulated by adding a Gaussian distributed error to the y-signal used by the PD regulator which determines the needed deflection angle (β), see equation (4). The magnitude of the standard deviation of the error is given by a percentage of the measured range. The larger the standard deviation is, the more incorrect the measured values used by the PD regulator become and consequently the more unsurtain the needed deflection angle becomes. A number of accelerometers is assumed to provide measured accelerations at different spanwise positions along the blade corresponding to the position of the flap section. By integrating these accelerations the overall blade deflection is found. Strain gauges are also assumed to be placed along the blade as an indicator on how much the measured acceleration is drifting. It is the assumption that there is a correlation between the measured strains at given points along the blade and the overall range of the blade deflection.

2.7 Wind model

For modeling the wing the Danish Standard DS472 [13] suggests the 3D turbulent wind of Veers[14]

using a turbulence intensity of 10%. The average wind speed used for the computations in the present work is 10m/s. Based on a constant rotational speed of 19.8 rpm, 15 rotationally sampled time series have been generated. Each of the 15 series corresponds to a radial position on the blade where the aerodynamic calculation point is located. The effect of tower shadowing and wind shear is implemented as described by Hansen [15].

3 Results

The potential for fatigue load reduction for the aeroservoelastic system will be analyzed in different stages.

First, different investigations of the optimum radial positions of the flapping sections are performed using ideal flaps. In this regard, an ideal flap is a flap with no restrictions on power consumption, with no time lag in the control system and with no noise on the signal used for controlling the flap.

Secondly, the implications of non-ideality of the flaps, i.e. limited actuator power, time lag, and signal noise in the control system, are investigated.

3.1 One meter ideal flap

The spanwise width of the six installed flaps, shown in Figure 1, was changed to one meter each. By flapping the sections one by one it was found that the optimum position for a one meter ideal flap is close to $r/R=0.9$. This position of the flap gives a 14% reduction in equivalent load for the flapwise root moment (EQ_F), see Figure 3.

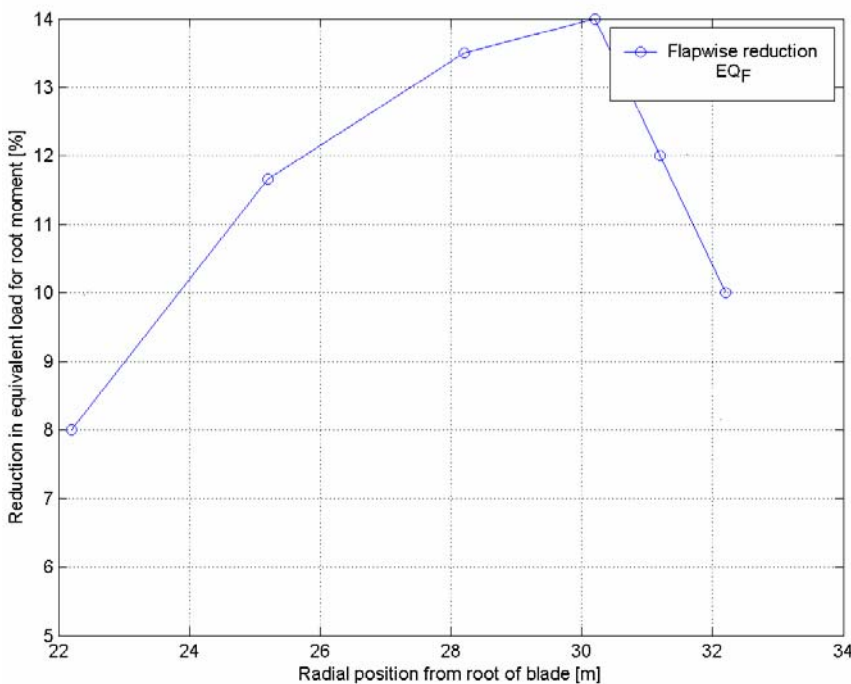


Figure 3: Equivalent load for the flapwise root moment using a one meter flap located at different radial positions on the wing.

The EQ_F curve in Figure 3 is proportional to the product of the chord times the relative wind velocity square.

3.2 Undivided large ideal flap

Allowing several neighbouring sections to flap at the same time forms a large continuous spanwise flap. Each of the sections comprising the large flap is allowed to deflect the flap independently. Figure 4 show the obtained EQ_F reductions as function of the length of the flaps. The radial placement of the flaps is given in the figure.

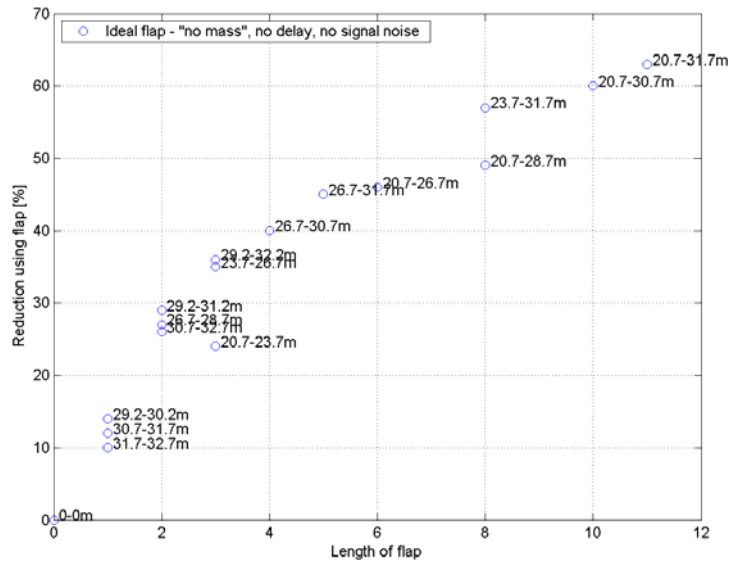


Figure 4: EQ_F for undivided large spanwise flaps as function of the spanwise length of the flap.

It is seen that the additional reduction in EQ_F decreases as the length of the flapping section is increased, and that the optimum placement of the undivided flapping section agrees well with what was expected from the results in Figure 3. It is seen from Figure 4, that a 11 meter flap gives an EQ_F reduction of more than 60%.

3.3 Divided ideal flaps

Instead of using one long continuous flap, several divided flaps were used simultaneously. Figure 5 illustrates the result of this investigation.

As seen from the results in Figure 5, higher reductions of the unsteady loads are possible for a given spanwise length of the flaps if the flap is not continuous. For instance 50% EQ_F reduction is possible using only 4 meters of flap in total. Compared to the undivided flap with a 40% EQ_F reduction, this is a relative increase of 25 %. The flapping part of the wing is in this case placed between 24m and 27m radius in combination with 31m to 32m radius.

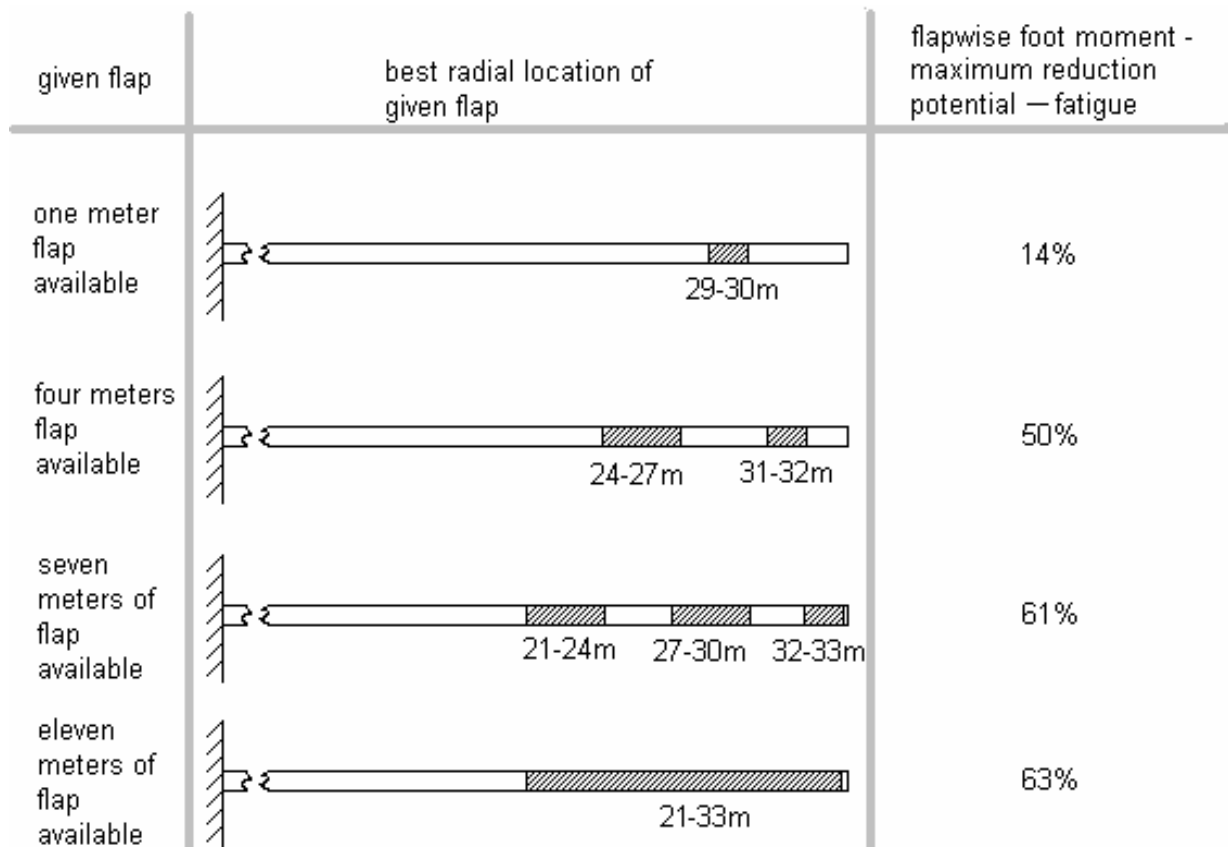


Figure 5: Optimum placement of various flap arrangements.

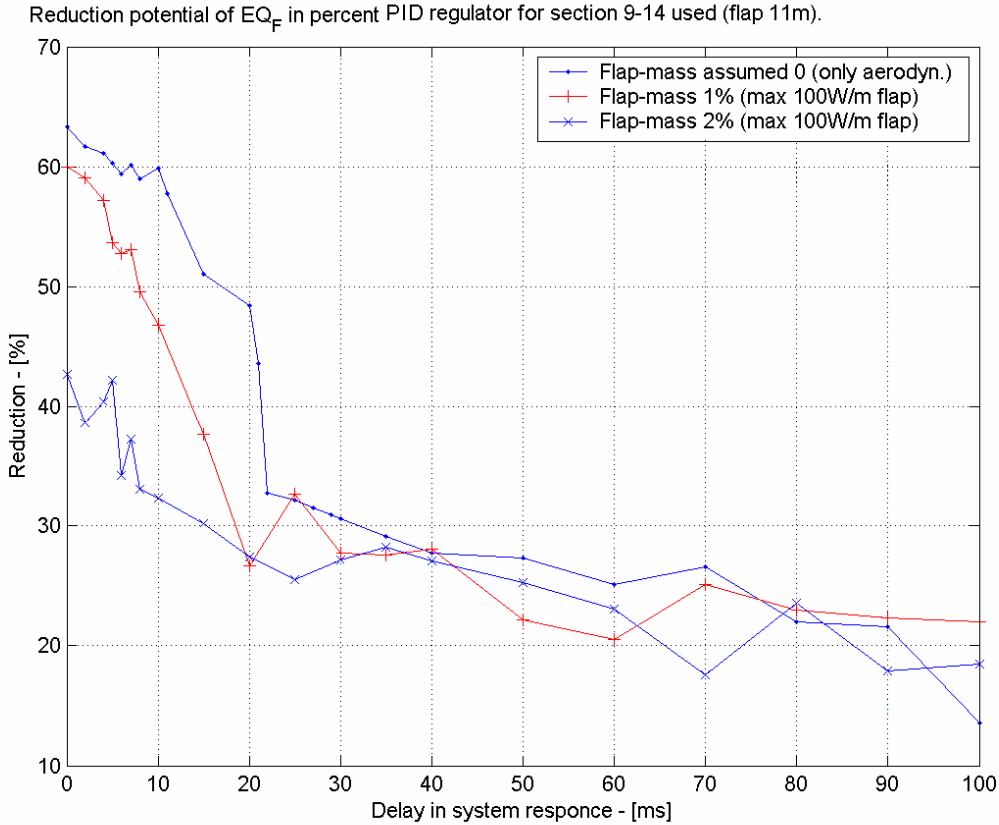


Figure 6: Flap actuator 100W/m, with finite flap mass. EQ_F is shown as function of control algorithm time lag for flap masses of 0%, 1% and 2% of the local sectional mass.

3.4 Limited actuator power and time lag in control system

When limited power is available for the flap actuator, the response time for the flap will decrease. The power needed by the flap actuation should balance out the power due to inertial forces and the power due to aerodynamic forces, as expressed in equation (5). The PID power regulator, given by equation (7), is tuned using a simple gain optimisation method described by Andersen [4].

A parameter study showed that the power needed by the flap actuator to balance the inertial forces of the flap motion is somewhat larger than the power needed to overcome the aerodynamic forces around the airfoil and in the wake. Therefore, an obvious remedy for decreasing the flap response time is minimizing the mass of the flap. The parametric study initially focused on keeping the response time for the flaps constant, however, limiting the overall power consumed by the flap actuators had to be taken into account if the system would ever have a commercial breakthrough. Several combinations of maximum available power for the TE flaps and different flap weights given as a percentage of the blade cross sectional weight was investigated and is shown in table 1.

Mass [%]	Max power [W/m]	Response time [ms]
10	± 1000	30-50
5	± 400	25-40
2	± 100	15-30
1	± 50	12-25
0.5	± 50	10-20

Table 1: Response time and power supplied for flaps.

In the first column the flaps have different weights given by a percentage of the cross sectional weight of the blade at the radial position of the flap.

Keeping the maximum available power constant at 100W/m, the weight of the TE flap and the general delay in response time was investigated. The general system response delay is defined as the time it takes a computer to collect and process the needed data until the flap actuators are feed backed. Comparing the EQ_F reduction potential for flaps weighing 0%, 1% and 2% of the cross sectional airfoil mass in combination with a general time lag the result is shown in Figure 6.

Figure 6 illustrates the importance of keeping the flap fairly light to prevent initial forces from making the flap respond slowly. At 0ms in general response delay the difference between a 1% flap-mass and a 2% flap-

mass is 16% EQ_F . Figure 6 shows the importance of keeping the general system response delay as small as possible. Delays in system response larger than 20ms severely limit the fatigue load reduction potential. Including 20ms time delays in system response gave a 30% reduction in efficiency for the 11 meter continuous flap with a flap mass of 1% of the local spanwise mass. Using flap-masses of two percent instead of one percent decreased the reduction potential by 15-20% for the fatigue in the flapwise blade root moment with identical power consumption for the flap actuators.

3.5 PD versus P control

A PD control was compared to a more simple P control. Spanwise flap lengths of 4, 7 and 11 meter have been investigated. The flaps are placed at the optimal radial positions given in section 3.3. The result of using PD and P regulators are shown in Table 2.

Regulator	4m flap	7m flap	11m flap
PD	46%	54%	60%
P	21%	23%	27%

Table 2: The reduction potentials in EQ_F obtained by using PD and P regulators.

A flap-mass of 1% and a maximum flap actuator power of 100W/m are used. Table 2 shows that it is important to include the differential gain for the regulator, as it roughly doubles the reduction potential.

3.6 Signal noise

From the dynamic blade model the actual flapwise deflection and derivatives is know for each time step. The control of the flap actuator has so far been based on the exact sectional flapwise blade deflections. Now imaginary accelerometers is placed near the flaps, to simulate actual measurement of the flapwise blade accelerations. The final design will have to take all fictitious forces into account. To compensate the simulated drift in flapwise deflection measured using the accelerometers a series of strain gauges is placed along the blade in an attempt to find the flapwise deflection using a correlation between strain and deflection. How this should be performed in reality still remains to be investigated. It is assumed that the sectional flapwise accelerations are measured by the fictitious accelerometers and the sectional flapwise deflections are found using a transformation of the measured strains along the blade. The aim of putting together this system of gauges is to see which effect Gaussian signal noise will have on the fatigue reduction potential. Gaussian signal noise of 5% Full Scale (FS) for the simulated accelerometer signal and 0.1% to 0.5% for the strain gauge signal has been

used. The result is shown in Table 3, where 11 meters of mass-less flaps is used.

Strain gauge error [% std.dev]	Accelerometer error [% std.dev]	EQ_F [%]
0.1	5	58
0.5	5	40

Table 3: Reduction in EQ_F using different control gains and adding signal noise (FS) to the feed signal.

4 Conclusion

For a one meter ideal flap, the optimum spanwise position to place the flap is at $r/R=0.9$. Using an 11 meter long ideal flap gives a significant reduction in fatigue loads for the flapwise blade root moment, when applying a 10 minute turbulent time series with 10% turbulence intensity, 10m/s average wind and wind spectral parameters suggested by DS472[13].

Dividing the flaps gives an increased efficiency of the flaps for a given spanwise flap length. A four meter continuous ideal flap gives a 40% reduction in flapwise equivalent root moment. However, dividing the 4 meter ideal flap in a 3 meter and a 1 meter flap, increase the reduction potential from 40% to 50%. Using 7 meter ideal flaps divided into two separate 3 meter flaps and one 1 meter flap increases the reduction potential from 50% to 61%.

Including 20ms time delays in system response gives a 30% reduction in efficiency for the 11 meter continuous flap with a flap mass of 1% of the local spanwise mass. Using flap-masses of two percent instead of one percent decreases the reduction potential by 15-20% for the fatigue in the flapwise blade root moment with identical power consumption for the flap actuators.

Using a PD regulator instead of a P regulator will make the flaps roughly twice as efficient.

Combining the signal from an accelerometer which has 5% signal error, with a strain gauge, the error in standard deviation for the strain gauge can be increased to 0.5% without loosing the fatigue reduction potential of the flapwise root moment for the blade.

Several ingredients have to be present in order to gain close to optimal reduction potential. The most sensitive parameters are: time delay, signal noise and spanwise installation of flaps.

Based on the investigations in this work it is concluded that the potential of using varying TE geometry for fatigue load alleviation on a wind turbine

blade is substantial.

Acknowledgement

It is gratefully acknowledged that part of this work is funded by the Danish Research Council through the Adapwing project.

Several Master Thesis projects were formulated in cooperation with Technical University of Denmark DTU-MEK as part of the ADAPWING project, see the work of Basualdo [16], Troldborg [17] and Andersen [4].

References

-
- [1]. Larsen, T., Madsen, H.Aa., Thomsen, K., April 2004, "Active Load Reduction Using Individual Pitch Based on Local Flow Measurements". Proc. EWEA The Science of Making Torque From Wind, Delft, Netherlands.
 - [2]. Bossanyi, E., April 2004, "Developments in Individual Pitch Control". Proc. EWEA The Science of Making Torque From Wind, Delft, Netherlands.
 - [3]. Buhl, T., Gaunaa, M., Bak, C., October 2005, "Potential Load Reduction Using Airfoils With Variable Trailing Edge Geometry", Journal of Solar Energy Engineering.
 - [4]. Andersen, P.B., Aug 2005, "Load Alleviation on Wind Turbine Blades using variable Airfoil Geometry (2D and 3D study)," Master Thesis, Technical University of Denmark, Department of Mechanical Engineering, Fluid Mechanics.
 - [5]. Hansen, M.O.L. dec 1999, "Aerodynamics of Wind Turbines", ISBN: 1-902916-06-9, James James (Science Publishers) Ltd.
 - [6]. Bramwell, A.R.S, Dec. 1999, "Helicopter Dynamics", ISBN: 0713133538, Edward Arnold (Publishers) Ltd.
 - [7]. Snel,H., Schepers, 1995, "Joint investigation of dynamic inflow effects and implementation of an engineering method", report number: ECN-C--94-107, ECN Solar and Wind.
 - [8]. Hansen, M.O.L., 2003, "Simulation of dynamic systems", Course notes on "41322 Aeroelasticity for windturbines", Technical University of Denmark.
 - [9]. Hansen, M.H., Juni 2000, "Modalanalyse er et effektivt værktøj til vingeafprøvning", Risø.
 - [10]. Øye S., 4/3 2003, "Dynamic model for elastic beams" handwritten notes. Denmark's Technical University.
 - [11]. Theodorsen, T., "General Theory of Aerodynamic Instability and the Mechanism of Flutter", NACA Report 496, 1935.
 - [12]. Kenschke, C.W. Soker,H., "Measurement of mechanical loads", International Standard IEC TS 61400-13 guidelines.
 - [13]. DS472, 1986, "Dansk Ingeniørforenings og IngeniørSammenslutnings Norm for Last og Sikkerhed for Vindmøllekonstruktioner," 1. udg. Danish Design Code for Wind Turbines (DK).
 - [14]. Veers P.S., March 1988, "Three-Dimensional Wind Simulation" Sandia Report Sand88-0152*UC-261 Unlimited release. United States Department of Energy.
 - [15]. Hansen, M.O.L., 2003, "Unsteady BEM", course notes on "41322 Aeroelasticity for windturbines", Technical University of Denmark.
 - [16]. Basualdo, S, Feb. 2004, "Load Alleviation on Wind Turbine Blades using variable Airfoil Geometry (A Two-Dimensional Analysis)," Master Thesis, Technical University of Denmark, Department of Mechanical Engineering, Fluid Mechanics.
 - [17]. Troldborg, N., May 2004, "Computational Study of the Risø -B1-18 Airfoil Equipped with Active Controlled Trailing Edge Flaps," Master Thesis, Technical University of Denmark, Department of Mechanical Engineering, Fluid Mechanics.
 - [18]. Gaunaa, M. 2005, "Unsteady 2D Potential-flow Forces on a Variable Geometry Airfoil Undergoing Arbitrary Motion", Technical report – Risøe-R-1478(EN). To appear..